Equilibrium properties of binary and ternary metallic immiscible nanoclusters

Abdiravuf A. Dzhurakhalov* and Marc Hou
Physique des Solides Irradiés et des Nanostructures CP234, Université Libre de Bruxelles, Boulevard du Triomphe, B-1050 Bruxelles, Belgium

(Received 14 April 2007; revised manuscript received 8 June 2007; published 30 July 2007)

Metropolis Monte Carlo free energy minimization in the (*NPT*) canonical ensemble is used to predict at the atomic scale the configurations of isolated metallic clusters made of two and three metals that are immiscible in the bulk. Clusters studied are formed by 200–1300 atoms by combining cobalt, silver, and copper. An embedded atom model potential is used to describe their cohesion. It is found that not only binding and interfacial configuration energies govern the composition of atomic configurations, but also thermal vibrational entropy plays a substantial role in the balance of energy contributions to thermodynamic equilibrium. Core-shell Ag-Co, Ag-Cu, and "onionlike" Cu-Co equilibrium configurations are found, which can be tuned by monitoring the interplay between composition and temperature. In ternary clusters, Ag always forms the surface layer and it is found that the Co and Cu distributions in the core depend on the Ag layer thickness.

DOI: 10.1103/PhysRevB.76.045429 PACS number(s): 61.46.Bc, 36.40.Mr, 68.35.Dv, 61.46.−w

I. INTRODUCTION

Metallic nanoparticles attract much interest because of the electronic, magnetic, optical, and catalytic properties that significantly differ from those of their bulk counterpart. Moreover, the possibility of tuning their size, morphology, structure, and composition opens routes to monitoring their properties in view of their application in nanoscale devices. Many of their properties are reviewed,[1–3] and several progress reports reveal that open questions are still numerous.[4,5] Experimentally, the advent of laser ablation cluster sources[6,7] promoted significant steps forward as they allow the synthesis of clusters, made of different chemical species, outside thermodynamic equilibrium. Mass selected cluster beams can be formed. Clusters then can be analyzed on the fly[8,9] or after deposition or codeposition on a substrate[10,11] using diffraction and direct observation with atomic resolution.

The understanding of cluster properties was boosted by the advent of the density functional theory[12,13] and the use of the local density approximation.[14] Such approaches are particularly efficient in the case of clusters formed by a limited number of particles as they allow correlating directly electronic, magnetic, and structural properties. When the number of particles is large or when observable properties result from statistics over large sets of configurations, classical mechanics grounded on semiempirical cohesion models proves to be realistic.

The possibility of characterizing clusters at the atomic scale experimentally and the available modeling tools at present motivates combining the approaches in order to gather understanding beyond the possibilities of uncorrelated studies. This is illustrated by progress in the accurate characterization of the atomic scale structure of clusters deposited on a surface[15,16] and segregation effects in bimetallic clusters.[17]

The knowledge of properties of bimetallic clusters is still limited as compared to elemental clusters because of the difficulty of synthesizing them in controlled conditions. Significant progress is, however, achieved[17–21] and direct comparison with model predictions is now possible.[15,16,22–24] This way, structural properties were addressed[16] as well as segregation effects[17,25] and the formation of core-shell particles.[19,26]

Many modeling studies were carried out beyond presently available experimental possibilities, leading to predictions over a large range of sizes, composition, and thermodynamic conditions. The relevant computational methods may be classified into two branches, both being extensively used. One is molecular dynamics, which is used to study the structure and the thermodynamics of small elemental clusters[27–30] as well as of bimetallic clusters,[31–33] and the second is energy minimization, which encompasses global minimization using genetic algorithms,[34–39] basin hopping methods,[29,36,40] Metropolis Monte Carlo (MMC),[25,41–46] or free energy concentration expansion methods.[47–50] As small numbers of atoms are concerned, classical and quantum mechanical approaches are sometimes combined as well.[25,51–53] For the purpose of modeling slow processes like cluster growth, multiscale approaches are also designed.[54–58]

The literature about the modeling of trimetallic clusters is still sparse[51,52,59–61] although, in principle, ternary clusters can be synthesized with the available experimental technologies.[62] However, such systems allow still much larger varieties of clusters as compared with binary systems, and thus, open the way to a still much larger variety of properties.

The purpose of the present study is to investigate the structural and thermal properties of binary and ternary metallic clusters systematically and to examine, where possible, the relationship between the properties of clusters made of two and of three different metals. In order to predict temperature dependencies, equilibrium clusters will be predicted by minimizing their Helmholtz free energy using a MMC algorithm.

We shall start from AgCo clusters already studied elsewhere in detail using a similar method[46] to which Cu will be added, which is miscible neither with Ag nor with Co. Characterizing first the temperature and composition dependencies of the structures of the AgCo, AgCu, and CoCu systems, their relationship with temperature and composition depen-

TABLE I. The parameters (Ref. 66) used in Johnson's functionals. α, β, and γ are dimensionless and determined from the atomic volume Ω, the cohesive energy E_c, the unrelaxed vacancy-formation energy E_{UF}, the bulk modulus, the Voigt-average shear modulus, and the equation of state of Rose *et al.* (Ref. 68).

Atom	Ω (Å^3)	E_c (eV)	E_{UF} (eV)	α	β	γ
Ag	17.10	2.85	1.10	5.92	5.96	8.26
Cu	11.81	3.54	1.30	5.09	5.85	8.00
Co	11.07	4.39	1.46	5.25	6.97	9.29

dencies of the AgCoCu system will be examined and discussed.

The paper is organized as follows. The MMC method will be briefly recalled in Sec. II and will be discussed in more detail within the present context. Section III is devoted to the discussion of the three binary systems AgCo, AgCu, and CoCu; Sec. IV is devoted to the AgCuCo system. A conclusion is presented in Sec. V.

II. MODEL

Binary and ternary clusters are studied as functions of their size, composition, and temperature, within realistic ranges. The size range considered is from 200 to 1300 atoms, which is a typical experimental range, with ideal truncated octahedral (TO) and spherical morphologies, with all stoichiometries and in the whole temperature range where they are in the solid state, and with emphasis on room temperature. The smallest cluster considered also corresponds to the smallest TO cluster with fcc structure. The number of atoms in a fcc cluster with TO morphology is given by[63]

$$N(n) = 16n^3 - 33n^2 + 24n - 6, \tag{1}$$

where n is an integer larger than 2. $n=2$, which is also possible, is a TO with a bcc structure.

In this paper, we restrict ourselves to clusters at thermodynamic equilibrium, and their minimal Helmholtz free energy configurations are predicted by Metropolis Monte Carlo. The technique is well documented,[64] and here we make use of its canonical (NPT) version where not only N but also the numbers of atoms of each element forming the cluster are kept constant. The sampling scheme includes two different trials; (i) random displacement of each atom in the cluster and (ii) random site exchanges of atoms of different species. Trials (ii) correspond to no physical path, but are used for limiting the risk of trapping the system into a local minimum as well as for enhancing convergence. Typically, 5×10^6 MMC steps involving both trials on each atom are used in each simulation. The main parameter which determines the minimal free energy state of the system is its configuration energy. Regarding the number of atoms in a cluster and the number of configuration energy estimates necessary in a MMC simulation, they are computed classically using a semiempirical potential. For modeling compounds, the embedded atom model[65] with the functional of the electronic density suggested by Johnson[66,67] is quite convenient as it allows the choice of the range of the atomic interactions. Indeed, the total configuration energy of a system is well known to be expressed by

$$E_T = \sum_{\text{bonds}} \Phi(r) + \sum_{\text{atoms}} F(\rho_a), \tag{2}$$

where the electronic density ρ_i at the site of atom i is written as

$$\rho_i = \sum_{j\neq i} f(r_{ij}), \tag{3}$$

where r_{ij} is the distance between atoms i and j. In Johnson's functionals, Φ and f are written as

$$f(r) = f_e\left[\frac{r}{r_1}\right]^{-\beta} \quad \text{and} \quad \Phi(r) = \Phi_e\left[\frac{r}{r_1}\right]^{-\gamma}, \tag{4}$$

where r_1 is the first neighbor distance and the scaling factors f_e and Φ_e are written as

$$f_e = \frac{E_c}{S_\beta \Omega} \quad \text{with } S_\beta = \sum_{i=1}^{n} \frac{N_i}{k_i^\beta} \tag{5a}$$

and

$$\Phi_e = \frac{2E_c}{S_\gamma} \quad \text{with } S_\gamma = \sum_{i=1}^{n} \frac{N_i}{k_i^\gamma}, \tag{5b}$$

where the summation runs over the n neighbor shells and N_i is the number of atoms in the ith shell. All parameters in Eqs. (2)–(5) are defined in Ref. 67 and are derived from the equation of state of Rose *et al.*[68] In this formalism, the number of shells, and thus the range of the interactions, is arbitrary.

For the purpose of the present simulations, shells until the fourth neighbor distance are used for the species having the largest first neighbor distance in its elemental equilibrium structure. Among Ag, Cu, and Co, it is Ag, which has a lattice distance at 0 K of 0.409 nm. The number of shells in the bulk fcc Cu and hcp Co is chosen such that the range of interaction is the same as in Ag. This way, the range of interaction involving atoms of different chemical natures is unambiguously the same. The parameters used are given in Table I, using Johnson's notations.

As the elemental solids are of concern, the potential is conveniently assessed, for instance, by comparing experimental and predicted thermal expansion coefficients and mean square thermal vibration amplitudes. In the case of compounds, the assessment is more delicate since Ag, Cu, and Co form no alloy in the bulk at equilibrium, for which

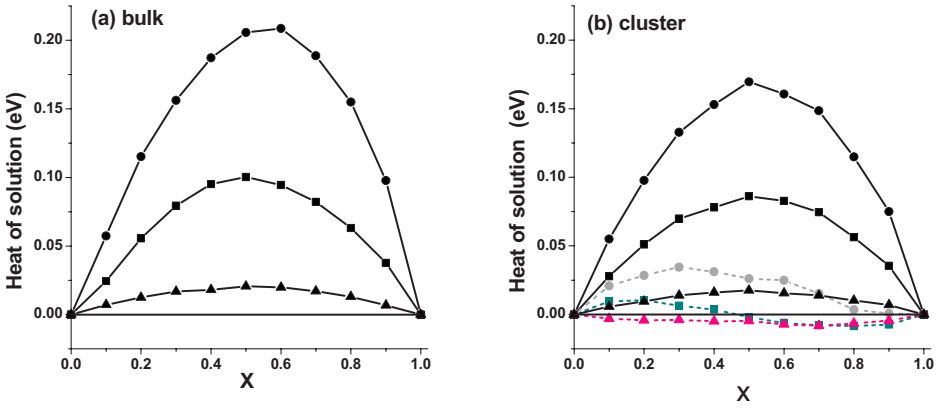

FIG. 1. (Color online) Heat of solution versus composition for $Ag_{1-x}Co_x$ (solid circles), $Ag_{1-x}Cu_x$ (rectangles), and $Cu_{1-x}Co_x$ (triangles) determined by MMC at $T=300$ K. Solid line, random distribution; dashed line, phase separated configuration. (a) Infinite solid; (b) 586 atom cluster.

similar properties could be measured. Using extended x-ray-absorption fine structure and Mössbauer spectroscopy data, it was, however, possible to assess the AgCo potential, and the approach of Johnson using weighted averages was found reasonable.[69] To our knowledge, such experimental data are not available for the AgCu and CoCu systems, and it is assumed that the same averaging technique still reasonably holds. This is supported by the computation of the heats of solution of the three Ag-Co, Ag-Cu, and Cu-Co systems versus composition and the comparison with experimental and theoretical studies of nonequilibrium alloys.

Artificial binary immiscible $Ag_{1-x}Co_x$, $Ag_{1-x}Cu_x$, and $Cu_{1-x}Co_x$ crystals were built with random spatial distribution of their compounds. Atomic positions were relaxed by MMC at 300 K, avoiding site exchange trials. Energy barriers were too high to allow for phase separation by trials on random atomic moves over millions of MMC steps. This way, the random distributions of the compounds were preserved in the simulations and the heat of solution of immiscible systems could be estimated versus composition. The results are depicted in Fig. 1(a). Consistently, the heat of solution is positive for all compounds with all stoichiometries, and the systems are thus correctly predicted immiscible with the potential used. The heat of solution of the $Ag_{0.5}Cu_{0.5}$ compound, 0.1 eV/atom, is consistent with previous estimates in the range of 0.065–0.12 eV/atom.[72–76] The fcc lattice parameter of the $Cu_{1-x}Co_x$ compound was measured by x-ray diffraction versus x.[77] The lattice parameters found using Johnson's potential at room temperature for the same compositions agree with these experimental values within 1 pm. Some doubt is, however, allowed regarding $Cu_{1-x}Co_x$ since, whatever the composition, the heat of solution is low and does not exceed 0.02 eV/atom. This magnitude is compared with the excess free energy of 0.06 eV/atom estimated in Ref. 77 for the unstable $Cu_{0.5}Co_{0.5}$ solid solution using the CALPHAD method.[78]

Therefore, in this case, an additional check was performed using a fcc infinite $Cu_{0.5}Co_{0.5}$ crystal in a MMC simulation at 300 K, allowing for site exchange trials. Atoms of each kind are initially distributed at random on the lattice. The numbers of Cu-Cu, Cu-Co, and Co-Co nearest neighbor (NN) pairs per atom were estimated as functions of the MMC step number. The results are shown in Fig. 2. In an ideally uniform binary solid solution, the number of mixed NN pairs per atom is twice that of homonuclear NN pairs of each kind. This is what is shown in Fig. 2 before the MMC minimization is started.

As the step number increases, the number of homonuclear NN pairs increases, while the number of mixed NN pairs decreases and they are found to converge to closer though nonidentical values, which is consistent with phases separated by an interface. Hence, the small positive heat of solution is sufficient to induce this phase separation.

Convergence is an issue in any minimization technique and, in the case of systems with a large number of degrees of freedom, like clusters, it is usually not possible to warrant that a global minimum of free energy is reached. For this reason, all MMC simulations presented in the following sections were repeated using different initial configurations. In many cases, like $Cu_{n-x}Co_x$ clusters, using initial core-shell configurations with either the Cu or the Co in the core, or using randomly distributed Cu and Co in the cluster, leads to the same final configurations, and these are retained for the discussions in Secs. III and IV. In others, like $Ag_{n-x}Co_x$, the same procedure leads to different configurations after 5×10^6 MMC steps. The corresponding configuration energies, however, differed significantly (typically by a few tenth of eV per atom). In such cases, the lowest energy configurations are retained for the discussion. Most generally, the lowest energy configurations found were also those for which the convergence of the algorithm was the most efficient.

III. BINARY CLUSTERS

Clusters deposited on a surface or embedded in a matrix often display facets, and ideal TO morphologies are privi-

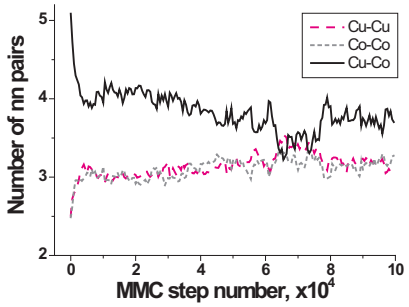

FIG. 2. (Color online) Mean number of nearest neighbor (NN) pairs per atom versus the MMC step number in the case of an infinite $Cu_{0.5}Co_{0.5}$ solid at 300 K.

TABLE II. Lattice distances, configuration, and surface energies of bulk Ag, Cu, and Co as predicted with the potential used. The comparison with available tight binding computations (Ref. 70) and experimental estimates (Ref. 71) is given.

	Ag	Cu	Co
a_0 (nm)	0.409	0.3615	0.3537
E_c (eV)	−2.85	−3.54	−4.39
Expt. γ (J/m^2)	1.25	1.83	2.55
γ_{100} (J/m^2)	2.07 (1.20[a])	3.12 (2.09[a])	3.25
γ_{111} (J/m^2)	1.90 (1.12[a])	2.97 (1.96[a])	3.02 (3.23[a])

[a]Reference 70.

leged for metals crystallizing in the fcc structure. Since Co also crystallizes in the fcc structure in nanoclusters, TO morphologies are here considered as privileged for bimetallic clusters too, made by combining two of the three elements Co, Cu, and Ag. Not only ideal TO morphologies are to be expected and, in order to assess the possible influence of faceting in the atomic configurations of binary clusters, they are predicted for both spherical and TO morphologies. Through all the results presented in this section and in the next one, except when mentioned, the morphology was not found to be of significant influence on atomic configurations. Therefore, the results and discussion are presented together.

Three different sets of clusters are considered, namely, $Ag_{n-x}Co_x$, $Ag_{n-x}Cu_x$, and $Cu_{n-x}Co_x$, with $n=201$, 500, or 586 and $0 \leqslant x \leqslant n$. $n=201$ and $n=586$ are the number of atoms in the two smallest ideal TO fcc clusters. Temperature was varied between 100 and 1000 K, however, most of the results depicted in this section are obtained at 300 K.

Figure 1(b) shows the heats of solution as functions of x for the 586 atom cluster, just as represented in Fig. 1(a) for bulk fcc crystals. Similar results are obtained with other cluster sizes. All heats of solution are found positive, demonstrating that, like in the bulk, Ag, Co, and Cu are also immiscible in nanoclusters. This is confirmed by repeating the MMC simulations, allowing for site exchange trials. The consequence is phase separation and, as shown in Fig. 1(b), the remaining excess energy is most reduced. When not vanishing, it is limited to the interfacial energy between the separated compounds.

The case of $Ag_{n-x}Co_x$ clusters was already examined in great detail elsewhere.[46] It was found that, in the solid state, the atomic configurations of both species result from a balance between lattice distortion and binding energy. When $x \leqslant 10$, it costs less energy to locate the Co atoms in small groups just beneath the surface and to displace the Ag surface atoms, therefore, then to regroup all Co atoms at the center of the cluster. At large x values, a core-shell structure with Co in the core is privileged. The question thus arises if this argument still holds for other immiscible compounds, and the cases of $Ag_{n-x}Cu_x$ and $Cu_{n-x}Co_x$ demonstrate that binding and relaxation are not generally sufficient to depict the whole energy balance, as will be shown now. Table II provides equilibrium lattice distances and energetic data for bulk Ag, Co, and Cu, as predicted with the interaction potential used.

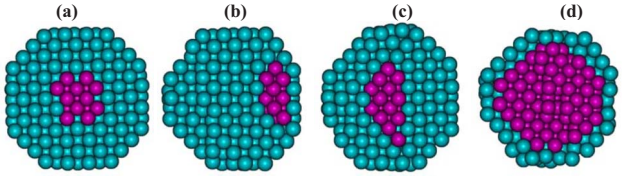

FIG. 3. (Color online) Cross sections of snapshots of TO $Ag_{586-x}Cu_x$ cluster at (a) $T=100$ K and $x=29$ (5% Cu), and at $T=300$ K and (b) $x=29$ (5% Cu), (c) $x=59$ (10% Cu), and (d) $x=293$ (50% Cu). Ag is in blue (light dark) and Cu in red (dark).

The case of $Ag_{n-x}Cu_x$ is still similar to $Ag_{n-x}Co_x$. In both cases, as shown in Table II, the configuration energy of bulk Ag is the highest and its bulk lattice parameter the largest. Atomic configurations of TO $Ag_{586-x}Cu_x$ are depicted in Fig. 3 for $29 \leqslant x \leqslant 293$. They are all core shell. When $x \leqslant 30$, like in $Ag_{n-x}Co_x$, copper forms small groups beneath the surface. The spatial organization depends on temperature, lower temperatures privileging a core-shell arrangement. In the case of the 201 atom clusters, a similar transition in configurations with x is also observed. At 300 K, it is found at $x \sim 15$.

The situation is more complex for $Cu_{n-x}Co_x$, which is now examined in detail. When $x \leqslant 10$, like in the previously discussed systems, Co is located close to the surface, but, here, it tends to form a uniform layer rather than a compact group. Slabs in a TO cluster with $n=586$ and $29 \leqslant x \leqslant 293$ are displayed in Fig. 4. There, it is seen that the Co does not agglomerate at the center of the cluster. It remains in the subsurface area and forms a homogeneous layer, the thickness of which increases with x. Such an "onion" structure was already predicted in a set of bimetallic clusters,[79] however, $Cu_{n-x}Co_x$ configurations are obtained here at thermodynamic equilibrium. Onionlike structures at thermodynamic equilibrium were already found, using similar MMC techniques as used in the present work, in icosahedral clusters containing up to 309 atoms, formed by copper and gold[43,44] as well as by palladium and platinum.[45] When the amount of Cu is not sufficient to form a full monoatomic overlayer, it is replaced by Co in {111} facets first, as shown in Fig. 4(e), and when its concentration is still lower, it is replaced in {100} facets and in edges next.

The reason why Cu forms a surface layer may be advocated to the fact that, as shown in Table II, the surface excess energies associated with {100} and {111} surfaces are lower than those of fcc cobalt. This was also found in macroscopic liquid Cu-Co droplets under microgravity conditions.[80] However, although the cohesion of bulk Co is stronger than that of Cu and its fcc lattice parameter is smaller, it does not form a single group at the cluster center like in $Ag_{n-x}Co_x$. In the case of $Ag_{n-x}Co_x$ and $Ag_{n-x}Cu_x$ clusters, surface energies, bulk cohesive energies, and lattice parameters consistently cause the core-shell configuration with the Co or Cu inside. Since these parameters do not suffice to explain the $Cu_{n-x}Co_x$ configurations the same way, one has to consider that the interfacial energy between Co and Cu may also enter into the balance. This one is, however, vanishingly small, as seen in Fig. 1(b). It is, moreover, hardly estimated in the case of the clusters considered because the layers involved are too thin

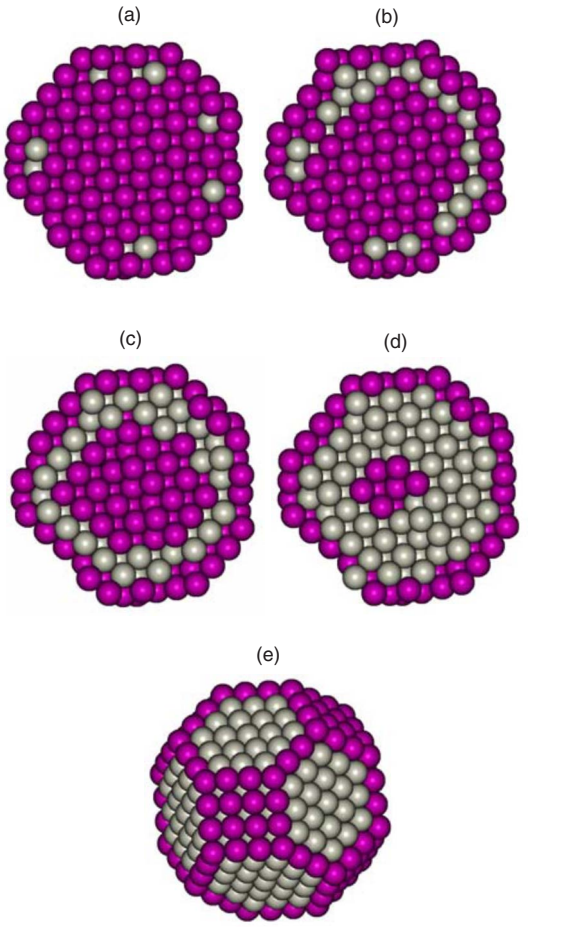

FIG. 4. (Color online) Cross section snapshots of TO $Cu_{586-x}Co_x$ cluster with 586 atoms at $T=100$ K: (a) $x=29$ (5% Co), (b) $x=118$ (20% Co), (c) $x=176$ (30% Co), and (d) $x=293$ (50% Co). (e) The whole cluster is represented for $x=469$ (80% Co). Co is in gray (light) and Cu in red (dark).

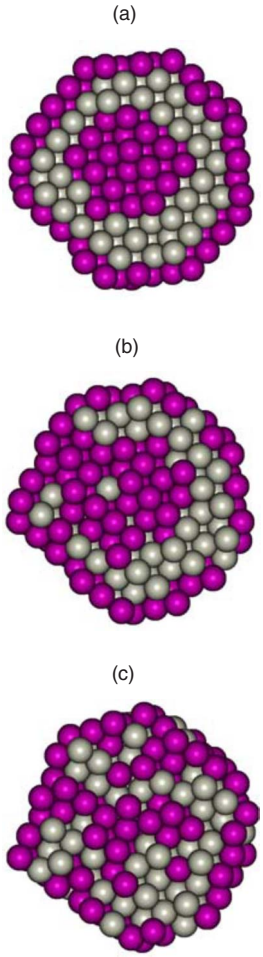

FIG. 5. (Color online) Cross section snapshots of TO $Cu_{586-x}Co_x$ cluster with $x=235$ (40% Co) at (a) $T=100$ K, (b) $T=300$ K, and (c) $T=500$ K. Co is in gray (light) and Cu in red (dark).

to reasonably factorize the various contributions to the total energy of the system. Configuration energy balances, as they can be made on the basis of Fig. 1 and Table II, do not account for the contribution of vibrational entropy to the Helmholtz free energy as minimized by the MMC algorithm. In the present case, its role is substantial. Indeed, the MMC minimization was repeated for several compositions, giving rise to the onionlike structure at different temperatures. Figure 5 illustrates the effect when the cluster contains 40% Co. In this figure, the equilibrium configuration of Co atoms in the onionlike cluster is shown at 100, 300, and 500 K. At 100 K, it is well ordered. The Co configuration displays the {111} and {100} facets of the TO geometry, just beneath the Cu surface layer. It is seen that, as the temperature increases, the Co layer gets disordered and, at 500 K, a significant amount of Co atoms are distributed at random within the core of the cluster and the onionlike arrangement is severely degraded. Hence, vibrational entropy unprivileges the onionlike arrangement.

One indirect method to emphasize the role of the interfacial energy is to tune it by means of an additional layer of atoms which would influence the energy balance of the Co-Cu subsystem. This is possible by adding Ag to $Cu_{n-x}Co_x$ clusters, and such ternary clusters are studied systematically in the next section.

IV. TERNARY CLUSTERS

$Ag_mCu_{n-x}Co_x$ ideal TO clusters are constructed with $m=385$ and $n=201$ ($m+n=586$) and $m=703$ and $n=586$ ($m+n=1289$), and minimal free energy configurations are predicted by MMC. In a first set of minimizations, x is varied at constant m and n in such a way that the amount of Ag is fixed and the relative composition in Co and Cu is varied. In a second set of simulations, the composition in Cu and Co is fixed and the amount of Ag is varied. Finally, in a third set, Ag is replaced by Cu and a binary system is modeled again. The effect of temperature is estimated by repeating the minimization at 100 and 300 K.

In addition to the use of snapshots, the analysis of configurations is carried out by means of radial density distributions, $g(r)$, obtained by averaging densities over configurations sampled within 5×10^5 MMC steps at equilibrium.

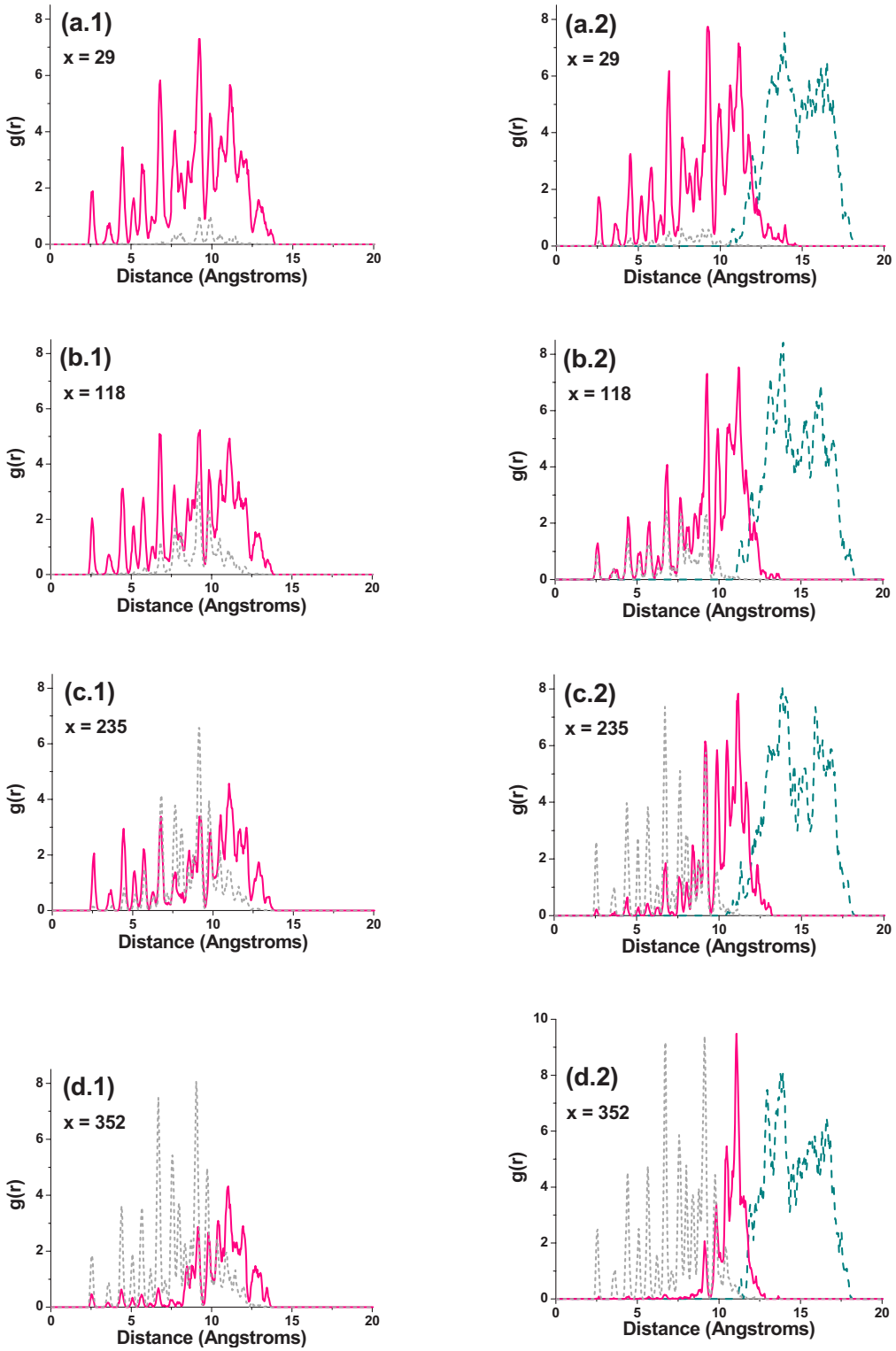

FIG. 6. (Color online) Radial distribution functions of components for binary $Cu_{586-x}Co_x$ clusters (left column) and ternary $Ag_{703}Cu_{586-x}Co_x$ clusters (right column) for the different concentrations of Co at $T=300$ K: (a) $x=29$ (5% Co in CuCo), (b) $x=118$ (20% Co in CuCo), (c) $x=235$ (40% Co in CuCo), and (d) $x=352$ (60% Co in CuCo). The functions are given distinctly for Co (dotted gray), Cu (solid), and Ag (dashed blue/dark).

Typical results at 300 K are shown in Fig. 6. In this figure, radial distributions in $Cu_{586-x}Co_x$ binary clusters and $Ag_{1289}Cu_{586-x}Co_x$ ternary clusters are compared. Snapshots of ternary clusters at equilibrium are shown in Fig. 7, providing illustrative detail at 300 and 100 K. Similar results were obtained with $m=586$ and $n=201$ clusters as well as at 100 K. In all cases, Ag forms the outer shell, consistently with its lower bulk cohesive energy, lower surface energy,

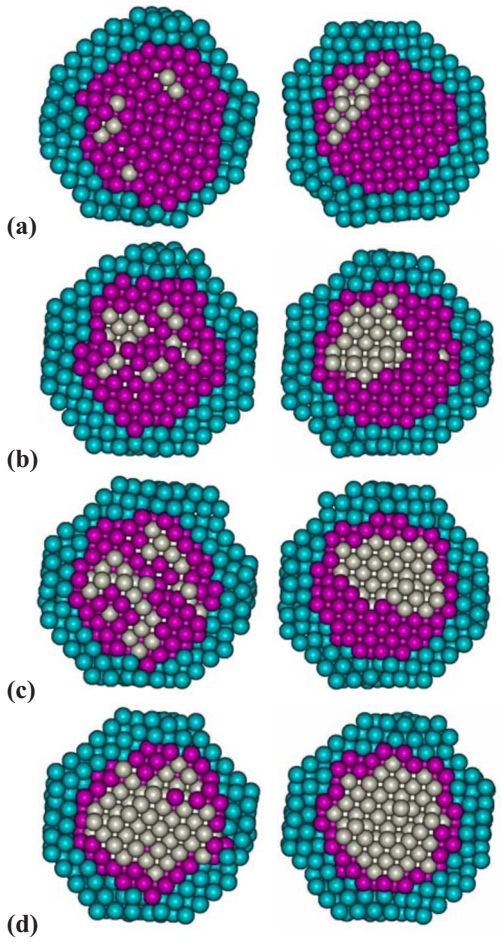

FIG. 7. (Color online) Cross section snapshots of TO $Ag_{703}Cu_{586-x}Co_x$ cluster with 1289 atoms at $T=300$ K (left column) and at $T=100$ K (right column). (a) $x=29$, (b) $x=118$, (c) $x=176$, and (d) $x=293$. Light gray, Co; red (dark), Cu; and blue (mid-gray), Ag.

and higher bulk lattice distance. In the cases of the lowest x values [Fig. 6(a1)], Co forms small groups close to the surface inside the binary $Cu_{n-x}Co_x$ cluster. In the ternary cluster with the same n and x [Fig. 6(a2)], such groups are not confined to the subsurface or interface area anymore and are distributed among the whole inner volume. It is only at the lowest temperature (100 K) that Co preferentially regroups beneath the Cu/Ag interface (Fig. 7). Hence, modifying the Cu surface energy by creating a Cu/Ag interface has a significant effect on Co distribution at small x. At intermediate x values [Fig. 6(b2)], the onionlike Cu-Co-Cu structure of the binary clusters does not occur anymore when a Ag layer is added, in which case, consistent with predictions that can be made on the basis of Table II, Co preferentially occupies the center, Cu forms an intermediate layer, and Ag forms the outer shell. Finally, at large x value [Fig. 6(d)], the Cu-Co core-shell structure is maintained when Ag is added to the system; however, the interface between the Co core and the surrounding Cu layer is sharper.

At 100 K, Co preferentially regroups (Fig. 7) and the positions of their groups depend on composition. At small x, it is located close to the interfaces, while it occupies the cluster center at larger x, similar to the case of binary clusters.

The role of the Ag outer shell can be appreciated in greater detail in $Ag_mCu_{n-x}Co_x$ clusters by keeping n and x constant and varying m. Results are exemplified in Fig. 8, showing radial distribution functions obtained with $n=586$, $x=118$, and $0 \leqslant m \leqslant 600$. When m is small, the onionlike structure of the binary cluster is preserved. As m increases, the mean radius of the Co layer decreases continuously until a Co-Cu mixture takes place, insensitive to any further increase of the Ag outer layer thickness, in the present case, for $m \geqslant 360$. Beyond this m value, the Ag/Cu interfacial energy is no longer influenced by a further increase of the Ag layer thickness.

The last aspect of the ternary cluster problem considered here is the identification of a possible balance between bulk cohesive energy and surface energy on the formation of the onionlike structure. In order to tackle this question, instead of adding Ag to a Cu-Co cluster of fixed composition, Cu is added. The results are depicted in Fig. 8 (right column), where radial density distributions are displayed for spherical $Cu_{468}Co_{118}Cu_m$ with $0 \leqslant m \leqslant 600$. When $m=0$, Co is distributed in the subsurface area according to the radial distribution in Fig. 8(a2). As seen in Figs. 8(b2), 8(c2), and 8(d2), increasing m has the effect of displacing the Co atoms outward without significantly altering the profile of its radial distribution. Moreover, the distance between the leading edges of the Co and Cu radial distributions is found independent of the amount of added copper. This clearly indicates that it is the cluster surface which governs the distribution of Co in the cluster. This contrasts with the effect of adding silver [Figs. 8(a1), 8(b1), 8(c1), and 8(d1)], where the Co distribution in Cu is governed by the Co/Ag interface.

V. SUMMARY

By using composition, temperature, size, and morphology as parameters, it was possible to show that the spatial arrangement of different immiscible species in binary and ternary compound clusters results from a complex interplay.

First, the competition between relaxation and binding energies determines whether a core-shell structure is thermodynamically stable or whether the species forming the tightest bonds will form small groups beneath the cluster surface. This question was already discussed in a previous work in the case of AgCo, which is found consistent with the case of AgCu discussed here. In the case of CuCo, where the differences in lattice spacing and in binding energies are smaller, surface excess energy plays an important role in the balance. The consequence of a lower Cu surface energy is the formation of a copper surface covering a Co layer, itself embedding a Cu core. Such a complex equilibrium "onionlike" structure seems, at first glance, inconsistent since Co is more tightly bound than Cu and would thus be expected to form the core. The role of the lower Cu surface energy in preventing this is evidenced by the role of an additional Ag layer in ternary clusters. According to its larger lattice spacing, its lower bonding energy, and its lower surface excess energy, at equilibrium, Ag forms the outer shell. As a consequence, the free Cu surface is replaced by a Cu/Ag interface and, con-

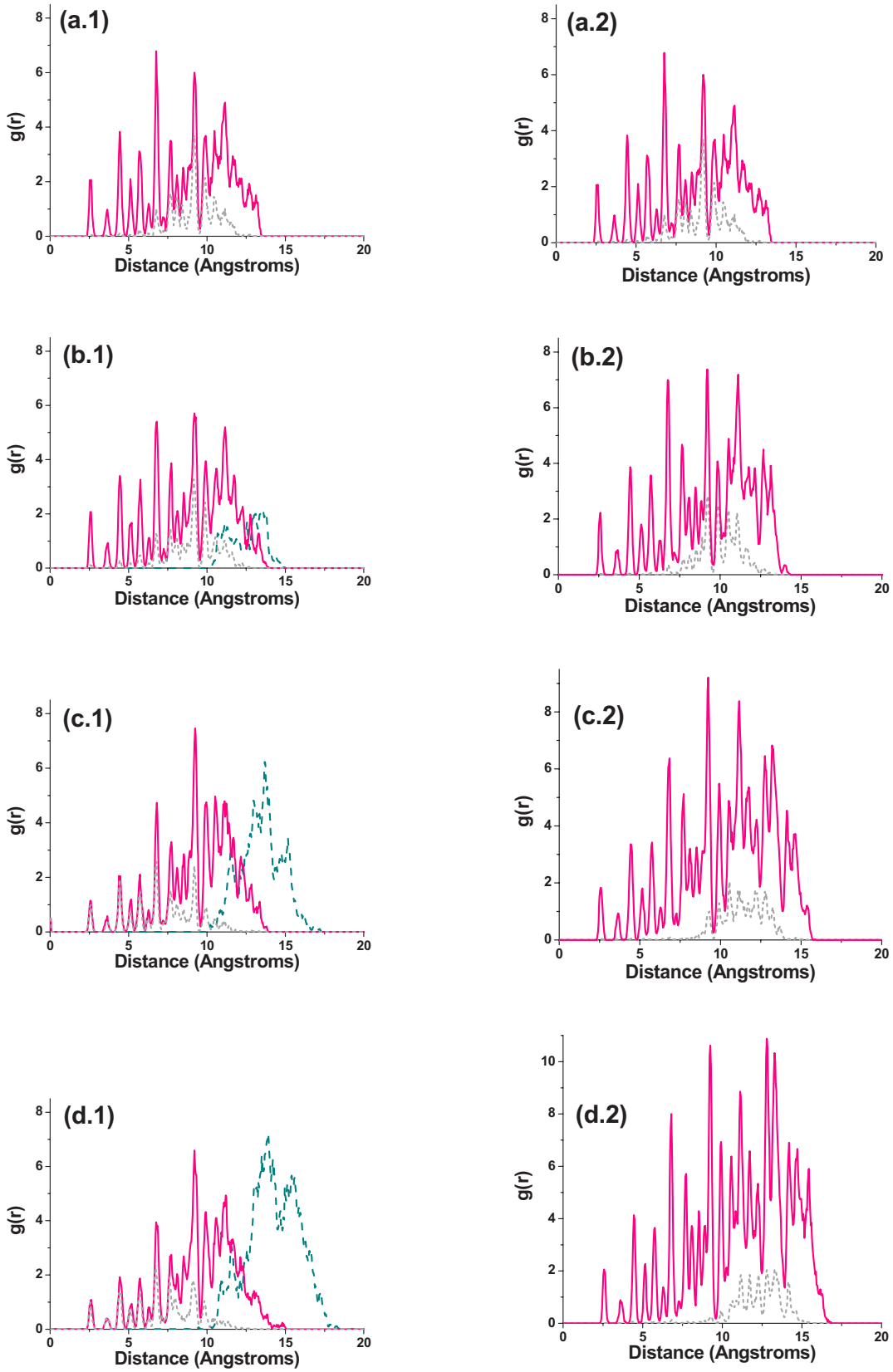

FIG. 8. (Color online) Radial distributions of $Ag_mCu_{468}Co_{118}$ clusters (left column) and $Cu_mCu_{468}Co_{118}$ clusters (right column) at $T=300$ K: (a) $m=0$, (b) $m=120$, (c) $m=360$, and (d) $m=600$. The line codes are the same as in Fig. 6.

sistent with the bonding criterion, Co moves to the core. Temperature is also at play by triggering the contribution of vibrational entropy to the Helmholtz free energy. The Cu-Co "onionlike" structure is sharpest at the lowest temperature. Increasing it modifies the energy balance, privileging the migration of Co from the interlayer to the cluster center. At a given composition, it also triggers the transition between small subsurface groups and core-shell configurations. In the range investigated, cluster size and morphology are not found to have a strong influence on these issues. Computer simulation results, thus, allow a comprehensive discussion of the interplay that governs the spatial distribution of the different compounds. Because of the semiempirical nature of the potential used however, a cross-check of predictions with experimental characterization is highly desirable. Characterizing spatial configurations of different species inside clusters experimentally is an arduous task. In addition, to our knowledge, no experimental technique allows such observations in isolated clusters with more than several tens of atoms. In so far as they may require bringing clusters to excited states, their temperature may not be under control, which, as comes out in the present study, would represent an important bias. The characterization of multicomponent clusters may be more realistic if they are supported on a surface or embedded in a matrix. Again, in this case, the present results indicate that the interface between a cluster and its environment may have a substantial influence on the spatial configuration of the species inside the clusters. In principle, such interfaces may be incorporated into the model, which would bridge the gap between model predictions and experiment.

ACKNOWLEDGMENTS

One of the authors (A.D.) is thankful for a grant of the Fonds National de la Recherche Scientifique of Belgium. This work was carried out under Research Agreement No. 2.4520.03F with the Fonds de la Recherche Fondamentale Collective.

*Corresponding author. FAX: 32-2-6505227; dzhurakhalov@mail.ru

[1] H. Haberland, *Clusters of Atoms and Molecules* (Springer-Verlag, Berlin, 1995).
[2] K. H. Meiwes-Broer, *Clusters on Surfaces* (Springer-Verlag, Berlin, 2000).
[3] L. W. Zhong, L. Yi, and S. Ze, *Handbook of Nanophase and Nanostructured Materials* (Kluwer Academic, New York, 2003).
[4] J. Bansmann, S. H. Baker, C. Binns, J. A. Blackman, J.-P. Bucher, J. Dorantes-Dàvila, V. Dupuis, L. Favre, D. Kechrakos, A. Kleibert, K.-H. Meiwes-Broer, G. M. Pastor, A. Perez, O. Toutlemonde, K. N. Trohidou, J. Tuaillon, and Y. Xie, Surf. Sci. Rep. **56**, 189 (2005).
[5] F. Baletto and R. Ferrando, Rev. Mod. Phys. **77**, 371 (2005).
[6] T. G. Dietz, M. A. Duncan, D. E. Powers, and R. E. Smalley, J. Chem. Phys. **74**, 6511 (1981).
[7] V. E. Bondybey and J. H. English, J. Chem. Phys. **74**, 6978 (1981).
[8] W. Bouwen, P. Thoen, F. Vanhoutte, S. Bouckaert, F. Despa, H. Weidele, R. E. Silverans, and P. Lievens, Rev. Sci. Instrum. **71**, 54 (2000).
[9] S. Neukermans, E. Janssens, Z. F. Chen, R. E. Silverans, P. v. R. Schleyer, and P. Lievens, Phys. Rev. Lett. **92**, 163401 (2004).
[10] M. Négrier, J. Tuaillon-Combes, V. Dupuis, P. Mélinon, and A. Perez, Philos. Mag. A **81**, 2855 (2001).
[11] P. Mélinon, V. Paillard, V. Dupuis, A. Perez, P. Jensen, A. Hoareau, J. P. Perez, J. Tuaillon, M. Broyer, J. L. Vialle, M. Pellarin, B. Baguenard, and J. Lerme, Int. J. Mod. Phys. B **139**, 339 (1995).
[12] P. Hohenberg and W. Kohn, Phys. Rev. **136**, B864 (1964).
[13] W. Kohn and L. J. Sham, Phys. Rev. **140**, A1133 (1965).
[14] R. Car and M. Parrinello, Phys. Rev. Lett. **55**, 2471 (1985).
[15] B. Pauwels, G. Van Tendeloo, W. Bouwen, L. T. Kuhn, P. Lievens, H. Lei, and M. Hou, Phys. Rev. B **62**, 10383 (2000).
[16] B. Pauwels, G. Van Tendeloo, E. Zhurkin, M. Hou, G. Verschoren, L. T. Kuhn, W. Bouwen, and P. Lievens, Phys. Rev. B **63**, 165406 (2001).
[17] P. Moskovkin, S. Pisov, M. Hou, C. Raufast, F. Tournus, L. Favre, and V. Dupuis, Eur. Phys. J. D **43**, 27 (2007).
[18] S. K. R. S. Sankaranarayanan, V. R. Bhethanabotla, and B. Joseph, Phys. Rev. B **71**, 195415 (2005).
[19] L. Favre, V. Dupuis, E. Bernstein, P. Mélinon, A. Perez, S. Stanescu, T. Epicier, J. P. Simon, D. Babonneau, J. M. Tonnerre, and J. L. Hodeau, Phys. Rev. B **74**, 014439 (2006).
[20] E. Janssens, S. Neukermans, H. M. T. Nguyen, M. T. Nguyen, and P. Lievens, Phys. Rev. Lett. **94**, 113401 (2005).
[21] E. Janssens, S. Neuckermans, X. Wang, N. Veldeman, R. E. Silverans, and P. Lievens, Eur. Phys. J. D **34**, 23 (2005).
[22] Q. Hou, M. Hou, L. Bardotti, B. Prével, P. Mélinon, and A. Perez, Phys. Rev. B **62**, 2825 (2000).
[23] L. Bardotti, B. Prével, P. Mélinon, A. Perez, Q. Hou, and M. Hou, Phys. Rev. B **62**, 2835 (2000).
[24] E. Janssens, T. Van Hoof, N. Veldeman, S. Neuckermans, M. Hou, and P. Lievens, Int. J. Mass. Spectrom. **252**, 38 (2006).
[25] J. L. Rousset, B. C. Khanra, A. M. Cadrot, F. J. Cadete Santos Aires, A. J. Renouprez, and M. Pellarin, Surf. Sci. **352-354**, 583 (1996).
[26] S. Rohart, C. Raufast, L. Favre, E. Bernstein, E. Bonet, and V. Dupuis, Phys. Rev. B **74**, 104408 (2006).
[27] R. C. Longo, C. Rey, and L. J. Gallego, Surf. Sci. **459**, L441 (2000).
[28] S. Özçelik and Z. B. Güvenç, Surf. Sci. **532-535**, 312 (2003).
[29] A. Sebetci and Z. B. Güvenç, Surf. Sci. **525**, 66 (2003).
[30] A. Sebetci and Z. B. Güvenç, Modell. Simul. Mater. Sci. Eng. **12**, 1131 (2004).
[31] B. Mierzwa, J. Alloys Compd. **362**, 178 (2004).
[32] J. L. Rodríguez-López, J. M. Montejano-Carrizales, and M. José-Yacamán, Appl. Surf. Sci. **219**, 56 (2003).
[33] S.-P. Huang, D. S. Mainardi, and P. B. Balbuena, Surf. Sci. **545**, 163 (2003).

[34] F. Baletto, C. Mottet, A. Rapallo, G. Rossi, and R. Ferrando, Surf. Sci. **566-568**, 192 (2004).
[35] C. Massen, T. V. Mortimer-Jones, and R. L. Johnston, J. Chem. Soc. Dalton Trans. **2002**, 4375.
[36] S. Darby, T. V. Mortimer-Jones, R. L. Johnston, and C. Roberts, J. Chem. Phys. **116**, 1536 (2002).
[37] G. Rossi, A. Rapallo, C. Mottet, A. Fortunelli, F. Baletto, and R. Ferrando, Phys. Rev. Lett. **93**, 105503 (2004).
[38] R. L. Johnston, Dalton Trans. **22**, 4193 (2003).
[39] J. P. K. Doye and D. J. Wales, Phys. Rev. Lett. **86**, 5719 (2001).
[40] J. P. K. Doye and F. Calvo, Phys. Rev. Lett. **86**, 3570 (2001).
[41] E. E. Zhurkin and M. Hou, J. Phys.: Condens. Matter **12**, 6735 (2000).
[42] L. Gómez, C. Slutzky, and J. Ferrón, Phys. Rev. B **71**, 233402 (2005).
[43] D. Cheng, S. Huang, and W. Wang, Phys. Rev. B **74**, 064117 (2006).
[44] D. Cheng, S. Huang, and W. Wang, Eur. Phys. J. D **39**, 41 (2006).
[45] D. Cheng, W. Wang, and S. Huang, J. Phys. Chem. B **110**, 16193 (2006).
[46] T. Van Hoof and M. Hou, Phys. Rev. B **72**, 115434 (2005).
[47] L. Rubinovich and M. Polak, Phys. Rev. B **69**, 155405 (2004).
[48] M. Polak and L. Rubinovich, Phys. Rev. B **71**, 125426 (2005).
[49] M. Polak and L. Rubinovich, Surf. Sci. **584**, 41 (2005).
[50] L. Rubinovich, M. I. Haftel, N. Bernstein, and M. Polak, Phys. Rev. B **74**, 035405 (2006).
[51] A. Bol, J. A. Alonso, J. M. López, and A. Mañanes, Z. Phys. D: At., Mol. Clusters **30**, 349 (1994).
[52] H. Oymak and S. Erkoç, Phys. Rev. A **66**, 033202 (2002).
[53] G. Barcaro, A. Fortunelli, G. Rossi, F. Nita, and R. Ferrando, Phys. Rev. Lett. **98**, 156101 (2007).
[54] H. Mizuseki, Y. Jin, Y. Kawazoe, and L. T. Wille, J. Appl. Phys. **87**, 6561 (2000).
[55] H. Mizuseki, Y. Jin Y. Kawazoe, and L. T. Wille, Appl. Phys. A: Mater. Sci. Process. **73**, 731 (2001).
[56] H. Mizuseki, K. Hongo, Y. Kawazoe, and L. T. Wille, Scr. Mater. **44**, 1911 (2001).
[57] K. Hongo, H. Mizuseki, and Y. Kawazoe, Mater. Trans. **42**, 439 (2001).
[58] K. Hongo, H. Mizuseki, Y. Kawazoe, and L. T. Wille, J. Cryst. Growth **236**, 429 (2002).
[59] A. Aguado and J. M. López, Phys. Rev. B **71**, 075415 (2005).
[60] A. Aguado and J. M. López, Phys. Rev. B **72**, 205420 (2005).
[61] A. Aguado and J. M. López, J. Chem. Theory Comput. **1**, 299 (2005).
[62] W. M. Fedosyuk, O. I. Kasyutich, and W. Schwarzacher, J. Magn. Magn. Mater. **198-199**, 246 (1999).
[63] R. Van Hardeveld and F. Hertog, Surf. Sci. **15**, 189 (1969).
[64] M. P. Allen and D. J. Tildesley, *Computer Simulation of Liquids* (Clarendon, Oxford, 1987).
[65] M. S. Daw and M. I. Baskes, Phys. Rev. B **29**, 6443 (1984).
[66] R. A. Johnson, Phys. Rev. B **39**, 12554 (1989).
[67] R. A. Johnson, Phys. Rev. B **41**, 9717 (1990).
[68] J. H. Rose, J. R. Smith, F. Guinea, and J. Ferrante, Phys. Rev. B **29**, 2963 (1984).
[69] M. Hou, M. El Azzaoui, H. Pattyn, J. Verheyden, G. Koops, and G. Zhang, Phys. Rev. B **62**, 5117 (2000).
[70] H. L. Skriver and N. M. Rosengaard, Phys. Rev. B **46**, 7157 (1992).
[71] F. R. de Boer, R. Boom, W. C. M. Mattens, A. R. Miedema, and A. K. Niessen, *Cohesion in Metals* (North Holland, Amsterdam, 1988).
[72] R. Najafabadi, D. J. Srolowitz, E. Ma, and M. Atzmon, J. Appl. Phys. **74**, 3144 (1993).
[73] T. Klassen, U. Herr, and R. S. Averback, Acta Mater. **45**, 2921 (1997).
[74] J. L. Murray, Metall. Trans. A **15A**, 261 (1984).
[75] G. Mazzone, V. Rosato, M. Pintore, F. Delogu, P. F. Demontis, and G. B. Suffritti, Phys. Rev. B **55**, 837 (1997).
[76] H. W. Sheng and E. Ma, Phys. Rev. B **61**, 9979 (2000).
[77] C. Gente, M. Oehring, and R. Bormann, Phys. Rev. B **48**, 13244 (1993).
[78] M. Haebe and T. Nishizawa, CALPHAD: Comput. Coupling Phase Diagrams Thermochem. **4**, 83 (1980).
[79] F. Baletto, C. Mottet, and R. Ferrando, Phys. Rev. Lett. **90**, 135504 (2003).
[80] I. Egri, J. Mater. Sci. **40**, 2239 (2005).